

## Pipe-flange detection with GPR

This article has been downloaded from IOPscience. Please scroll down to see the full text article.

2011 J. Geophys. Eng. 8 35

(<http://iopscience.iop.org/1742-2140/8/1/006>)

View [the table of contents for this issue](#), or go to the [journal homepage](#) for more

Download details:

IP Address: 157.92.44.71

The article was downloaded on 09/12/2010 at 16:19

Please note that [terms and conditions apply](#).

# Pipe-flange detection with GPR

Néstor Bonomo, Matías de la Vega, Patricia Martinelli and Ana Osella

Departamento de Física, Facultad de Ciencias Exactas y Naturales, Universidad de Buenos Aires, Ciudad Universitaria, Pabellón 1, 1428 Buenos Aires, Argentina

E-mail: [bonomo@df.uba.ar](mailto:bonomo@df.uba.ar)

Received 26 May 2010

Accepted for publication 27 October 2010

Published 9 December 2010

Online at [stacks.iop.org/JGE/8/35](http://stacks.iop.org/JGE/8/35)

## Abstract

This paper describes an application of the ground penetrating radar (GPR) method for detecting pipe flanges. A case history is described in which GPR was successfully used to locate pipe flanges along an 8 km metal pipeline, using a fixed-offset methodology, from the ground surface. Summaries of numerical simulations and *in situ* tests, performed before the definitive prospecting to evaluate the feasibility of detection, are included. Typical GPR signals are analysed and several examples shown. Constant-time sections of data volumes and migration are evaluated with the goal of distinguishing flange signals from rock signals in unclear situations. The applied methodology was effective for detecting the pipe flanges in relatively short times, with accuracies below 10 cm in the horizontal direction and 20 cm in the vertical direction.

**Keywords:** GPR, pipe-flange detection, non-invasive methods

## 1. Introduction

Pipe flanges are important points in a pipeline. Monitoring is often performed at these points to control the internal flux and to prevent leaks due to corrosion or fatigue. They are also relevant for maintenance and access to the interior of the pipelines. Nevertheless, on some occasions the positions of the flanges are unknown, as in old pipelines or when planes or signposts are missed. Then, in these cases, it is relevant to locate them.

During the last decade, the ground penetrating radar (GPR) method has been widely applied in very different areas of investigation, such as geology, hydrology, soil preservation and archaeology. For example, the GPR method has been used to detect and map shallow faults and cavities (Gomez *et al* 2009, Vanneste *et al* 2008, Deparis *et al* 2008, Delle Rose and Leucci 2010), to monitor liquids and gases in the subsoil (Soldovieri *et al* 2008, Pettinelli *et al* 2008, Arts *et al* 2008, Crocco *et al* 2009), to detect waste and landfills (Orlando and Marchesi 2001, Hermozilha *et al* 2009), to map archaeological dwellings, tunnels and burials (Bonomo *et al* 2009, Berard and Maillol 2008) and also to detect unexploded ordnance (Zyadaa *et al* 2009, Ho and Gader 2008, Soliman and Wu 2008). In the civil-engineering area, the method has been applied to detect and characterize foundations and other structures (Pérez-Gracia *et al* 2009, Masini *et al* 2010),

to inspect inclusions and different characteristics of concrete (Hugenschmidt and Kalogeropoulos 2009, Xie *et al* 2007), to detect fractures in materials (Orlando and Slob 2009, Leucci *et al* 2007) and to locate and characterize utilities (Al-Shuhail 2006, Pettinelli *et al* 2009, Borgioli *et al* 2008). However, the detection of pipe flanges with GPR has not been practically addressed in the literature.

Fixed-offset (or equivalently, single-offset, SO) ground-surface implementations of the GPR method make it possible to prospect large sections or volumes of soil in relatively short times, with good target resolution, penetration depth and positioning precision. For example, vertical resolutions of a few centimetres can be attained with radar frequencies of 1000 MHz, or a few tens of centimetres with 250 MHz. With the last frequency, depth penetrations as large as 5 m can be obtained, depending on the soil characteristics, GPR system and acquisition procedure. As a consequence, the SO methodology appears to be suitable for detecting pipe flanges in situations that include shallow, large-to-intermediate-diameter pipelines, such as water, hydrocarbon, mineral and gas pipelines. Moreover, this kind of methodology avoids removing the soil around the pipeline or altering its normal functioning, since it works from the ground surface in a non-invasive way.

In this paper we apply a SO GPR methodology to locate pipe flanges (figure 1) along an 8 km segment of a pipeline. We



**Figure 1.** A pipe flange similar to those we looked for.

summarize the main results of numerical simulations and field tests carried out prior to the prospecting in order to evaluate the possibility of detecting the flanges. Next, we present typical data sections and analyse the electromagnetic responses of the pipeline to establish the determining factors and limits of detection. Then, we describe the prospecting and give several examples in which flanges were detected. Finally, we analyse constant-time slices of data with the goal of distinguishing between signals from flanges and signals from rocks in unclear situations, as well as the results of applying migration to them.

## 2. Numerical simulations

In this section, we show the results of numerical simulations carried out before the field tests and definitive prospecting. We performed these simulations to evaluate the possibility of detecting the pipe flanges from the ground surface by acquiring consecutive fixed-offset survey lines along the pipeline. If effective, this methodology would optimize the acquisition and processing times in relation to other kinds of prospecting that include parallel SO survey lines, either along or across the pipeline, or variable-offset lines.

The investigated section of the pipeline was 8 km in length, with expected depths from the air–soil interface to the pipeline of between 0.5 and 1.5 m. The external diameter of the flanges  $d_f = 52$  cm, the width of the junction  $w_f = 20$  cm and the external diameter of the pipe  $d_p = 20$  cm (figure 2(a)). The pipeline is metallic, with a thin isolating coating around it. The surrounding soil presented a predominantly sandy composition, with relatively moderate contents of clays in a few segments of the pipeline trajectory. Low-humidity conditions for the soil, according to its characteristics and the regional climate, were expected.

During the preliminary evaluation we analysed which GPR frequencies were suitable for resolving the signals from the tops of the flanges and the pipe, in order to clearly distinguish between them in a simultaneous visualization. Under these conditions, in a real prospecting, it would be possible to directly identify the most probable flange signals and to disregard other similar signals (typically, those due to rocks) by analysing their shapes and time positions with respect to the pipe signal. According to the given flange and pipe diameters, a vertical resolution better than 16 cm had to be attained with the GPR waves in order to distinguish

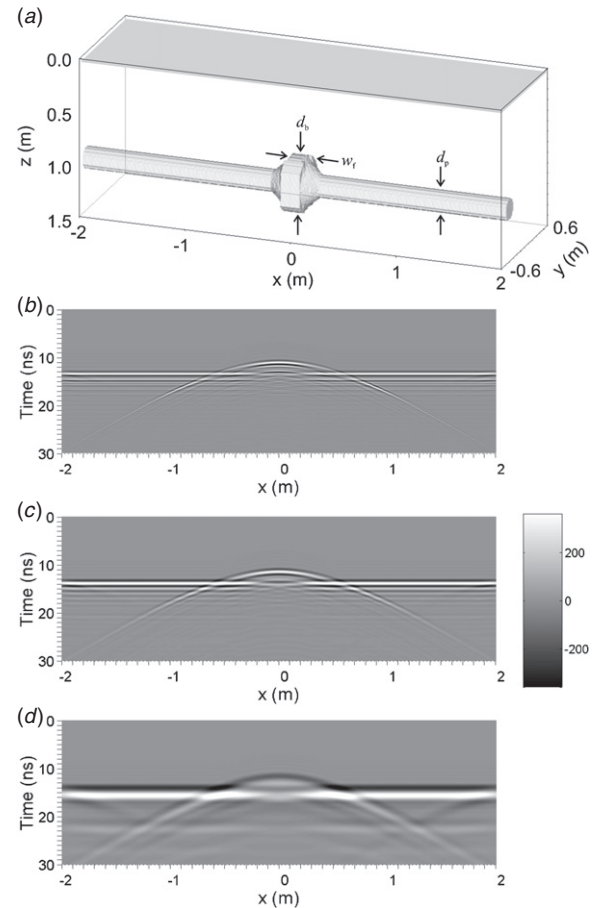


**Figure 2.** (a) Scheme of the investigated pipeline. The external diameters of the flanges and the pipe are  $d_f = 52$  cm and  $d_p = 20$  cm, respectively, the width of the junction is  $w_f = 20$  cm, whereas the expected depth of the pipeline varies from 0.5 to 1.5 m. The figure also corresponds to the model used to simulate the radargrams in (b)–(d). In this model, the pipeline is centred at a depth of 1.0 m and the velocity of propagation inside the soil is  $14 \text{ cm ns}^{-1}$ . (b) Simulated 1000 MHz profile for the model in (a); (c) 500 MHz profile; (d) 250 MHz profile.

between them. The theoretical (low-limit) estimations of the GPR vertical resolution for the most common GPR frequencies, 1000, 500, 250 and 100 MHz, and expected soil conditions (propagation velocities from 12 to  $16 \text{ cm ns}^{-1}$ , approximately; Reynolds 1997) are 3–4, 6–8, 12–16 and 30–40 cm, respectively. As a consequence, enough theoretical resolution only occurs for 1000 and 500 MHz, limit resolution for 250 MHz and insufficient resolution below this frequency.

We used Reflex-Win V.5.0.5 for the simulations, which calculate the fields through a finite-difference routine. A transverse-electrical polarization was considered in all cases. Figure 2(a) shows a typical model, in which the pipeline is embedded in a homogeneous half space at 1 m depth. The medium above the soil is air. The relative permittivity of the pipeline  $\epsilon_{rp} = 200$ , the relative permeability  $\mu_{rp} = 1$  and the conductivity  $\sigma_p = 99.99 \text{ S m}^{-1}$ . The pipeline permittivity has been assumed somewhat below the permittivity of metal ( $\epsilon_{rm} = 300$ , approximately, Zeng and McMechan 1997), due to the existence of the isolating coating. For the conductivity

of the pipeline, we have selected the highest value allowed by the software. As a general methodology, we checked the stability of the simulated data up to this conductivity, and within the permittivity interval of  $100 < \epsilon_{\text{TP}} < 300$ . On the other hand, the soil parameters of the model in figure 2(a) are as follows: relative permittivity  $\epsilon_{\text{rs}} = 4.6$ , relative permeability  $\mu_{\text{rs}} = 1$  and conductivity  $\sigma_s = 0.001 \text{ S m}^{-1}$  (propagation velocity  $14 \text{ cm ns}^{-1}$ ), which are typical values for the zone. The size of the model is  $4 \times 2 \times 1.5 \text{ m}^3$ , along the direction of the pipeline, across the pipeline and in the vertical direction, respectively, and the spatial increment is 1 cm in all directions. The time increment is 0.3 ns. We use an approximately sinusoidal waveform for the emitter, with a main minimum–maximum, and a subsidiary minimum–maximum after them.

Figures 2(b)–(d) show sections of the simulated data (offset = 0 m), for radar frequencies of 1000, 500 and 250 MHz, respectively. In all these cases, the profile lines are parallel to the pipeline and centred on the flange, with null lateral distance between the profile lines and the pipeline. Exponential gain has been applied in all cases. In general, the hyperbolic signals in the figures correspond to reflections at the flange, whereas the flat signals correspond to reflections at the pipe. The weaker half-hyperbolae arising at the left and right sides of figure 2(d) are due to border effects. For frequencies of 1000 and 500 MHz, figures 2(b) and (c), the signals of the flange and the pipe present comparable amplitudes and are clearly resolved in their central parts. Then, in an experimental situation, it is probable that both can be simultaneously visualized and distinguished. In the case of the 250 MHz frequency, figure 2(d), the flange signal presents a lower intensity than the pipe signal, whereas the central parts of both signals superimpose. As a consequence, in an experimental situation, it is not very likely that the signal of the flange can be distinguished from a direct visualization. Moreover, identification would be worse in a real situation because the signals of interest distort due to interference with the surrounding signals. Differentiation also complicates if the propagated frequencies are significantly below the nominal frequency of the antennae or if the wavelets present higher numbers of maxima. As a procedure to overcome the insufficient resolution, representative  $(x, t)$  pairs could be obtained along the pipe signal, the pipe signal filtered out, and the resulting data shown with the  $(x, t)$  points superimposed as references. Although this would make it possible to detect the flange signals, a greater complexity in the processing and analysis sequence is introduced, with significantly larger times involved.

Another objective of the prospecting, besides locating the flanges along the pipeline, was to measure their depths. A possible way to attain this objective was to fit hyperbolae to the probable flange signals, and then to obtain their depths from the parameters of the fits. Although this procedure does not *a priori* require any additional data (other than those acquired through the planned profiles), the resulting depths could be affected by involuntary deviations from the pipeline trajectory and the finite size of the flanges with respect to the GPR wavelengths. Fluctuations in the topography and the velocity

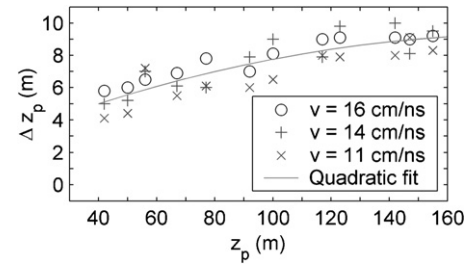


**Figure 3.** Difference between the fitted and model depths,  $\Delta z_p$ , as a function of the pipeline depth,  $z_p$ , for frequency  $f = 500 \text{ MHz}$  and different velocities of propagation  $v$ .

of propagation could also affect the resulting depths, as occurs with other GPR methodologies (e.g. fitting hyperbolae to transverse profiles or common midpoint analysis). It is clear that the magnitude of the difference between the results of the laterally deviated and not-deviated lines depends on the magnitude of the deviation and the depth of the pipeline. For example, for a lateral deviation of 20 cm and a pipeline depth of 50 cm, the fitted depth is 4 cm greater than the depth of a non-deviated profile, whereas for a lateral deviation of 40 cm and a pipe depth of 150 cm, the difference is 5 cm. These values indicate that a small amount of error is added to the depth due to this factor, provided that the lateral deviation can be kept below 20 cm.

The effects on the predicted depths of fitting hyperbolae to signals produced by non-punctual reflectors were estimated by simulating radar sections for different pipeline depths,  $z_p$ , frequencies,  $f$ , and velocities of propagation,  $v$ , fitting hyperbolae to the resulting flange signals and calculating the differences between the fitted and modelling depths  $\Delta z_p$ . As an example, figure 3 shows  $\Delta z_p$  as a function of  $z_p$ , for  $f = 500 \text{ MHz}$  and  $v$  as a parameter. The result of a second-order fit performed on the entire data set has also been included in the figure. The distribution of the data in the figure indicates a depth difference of around  $5 \pm 1 \text{ cm}$  for the expected minimum pipe depth, 50 cm, and  $9 \pm 1 \text{ cm}$  for the expected maximum, 150 cm. In general, the fitted values become increasingly larger than the values of the models for increasing pipe depths, with low dependences on the propagation velocity and frequency. Second-order curves as that shown in figure 3 were used to correct the fitted depths during the field tests and prospecting, in order to reduce the error in the vertical coordinates of the flanges.

### 3. Field tests

The field tests were designed on the basis of the numerical results summarized in the previous section and carried out before the definitive prospecting. They were performed at a sector of the pipeline where the positions of the flanges were known, and also at a few segments of the sector to be investigated. In the first case, we studied if the flanges could be satisfactorily detected and which were the relevant factors and limits of detection. In the second sector, we simply checked that the field characteristics were not significantly different from the first sector, and that the pipeline could be clearly visualized.

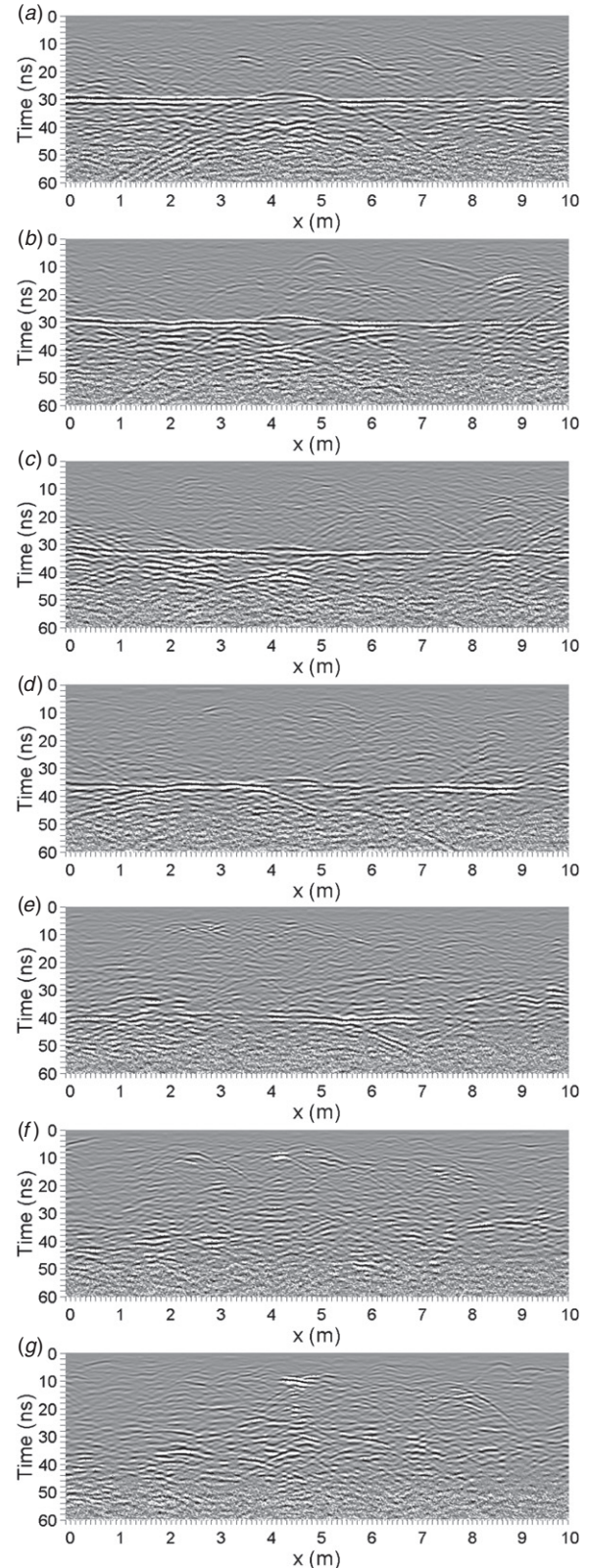
We used a Sensors & Software Pulse EKKO PRO system with 500 MHz antennae for the tests, which promised adequate resolution and penetration, and a direct visualization of the signals of the flanges and the pipe. We dismissed the 250 MHz frequency because of its limited resolution, as explained in the previous section, and the 1000 MHz frequency due to its low penetration, often below a metre, which was insufficient for many segments of the pipeline. A constant trace interval of 0.02 m was used, with stacking 16 in most of the tests. At the moment of the tests we measured a propagation velocity of  $13.1 \pm 2.0 \text{ cm ns}^{-1}$ , which was obtained by fitting hyperbolae to diffraction signals in the profiles. The processing steps that led to the figures are rubberbanding in the longitudinal coordinate, dewow, time-zero correction, removal of the direct waves between the antennae and application of exponential gain.

### 3.1. Lateral distance from the profile line to the pipeline

To analyse the effects of the lateral distance between the profile line and the pipeline on the amplitude of the signals, we acquired parallel lines at increasing distances from the pipeline,  $d$ , and analysed the results. In figure 4 we show a number of profiles with  $d$  increasing from 0 to 3 m, with an increment of 0.5 m. All the profiles were centred at the position of a flange.

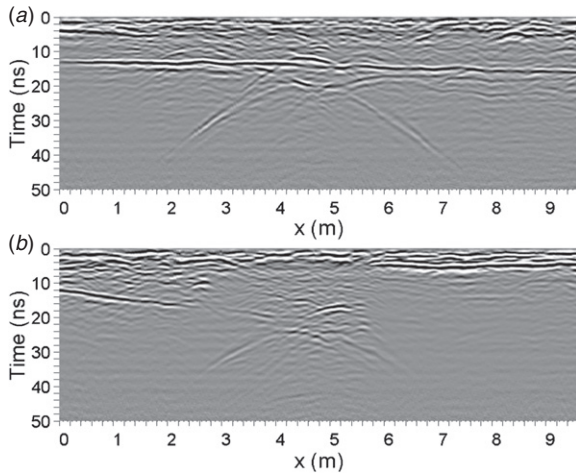
For  $d = 0 \text{ m}$ , figure 4(a), the signal of the flange can be clearly observed with vertex at  $(x, t) = (4.3 \text{ m}, 26 \text{ ns})$  and the signal of the pipe at  $t = 28.5 \text{ ns}$ , approximately. When the lateral distance is increased, figures 4(b)–(d), the signal of the flange becomes less clear. At an approximate distance  $d = 2 \text{ m}$  (figure 4(e)) the flange signal cannot be distinguished among the surrounding signals, and at  $d = 3 \text{ m}$  also the pipe signal has disappeared (figure 4(g)). This result indicates that the maximum lateral deviation from the GPR line to the pipeline during the prospecting should be below 1.5 m for pipeline depths of around 2.1 m. For larger  $d$ 's the pipeline signals are too weak to be detected because of the increasing wave paths and associated attenuation, and the directivity of the transmitted field.

Figure 5(a) shows a profile parallel to the pipeline, with  $d = 0 \text{ m}$  and centred at the position of a flange, whereas figure 5(b) shows a profile with the same origin as the previous one, but forming a non-zero angle with respect to the pipeline. The pipe and flange signals can be clearly identified in figure 5(a) for a not-deviated survey line. In contrast, in figure 5(b) the signal of the pipe attenuates and finally disappears when the lateral distance from the pipeline to the acquisition point increases, whereas the flange signal is hardly visible. It is clear that in the last case it would be rather improbable to recognize the flange signal during a real prospecting. This example shows that for a pipeline depth of around 1 m, the maximum lateral deviation from the GPR line to the pipeline has to be below 0.9 m in order to detect the flange signal. In general, from the analysis of these and other similar tests we obtained that the maximum lateral deviation from the pipeline to the survey line should be 0.6 m, in



**Figure 4.** A set of profiles parallel to the pipeline ( $f = 500 \text{ MHz}$ ), acquired at increasing distances  $d$  from it. A flange is located at  $x = 4.3 \text{ m}$ . (a)  $d = 0 \text{ m}$ ; (b)  $d = 0.5 \text{ m}$ ; (c)  $d = 1 \text{ m}$ ; (d)  $d = 1.5 \text{ m}$ ; (e)  $d = 2 \text{ m}$ ; (f)  $d = 2.5 \text{ m}$ ; (g)  $d = 3 \text{ m}$ .

order to detect the flanges at the minimum expected depths (0.5 m).



**Figure 5.** (a) Profile acquired along the pipeline, with  $d = 0$  m and centred at the position of a flange; (b) profile with the same origin as the previous one but forming a non-zero angle with the pipeline.

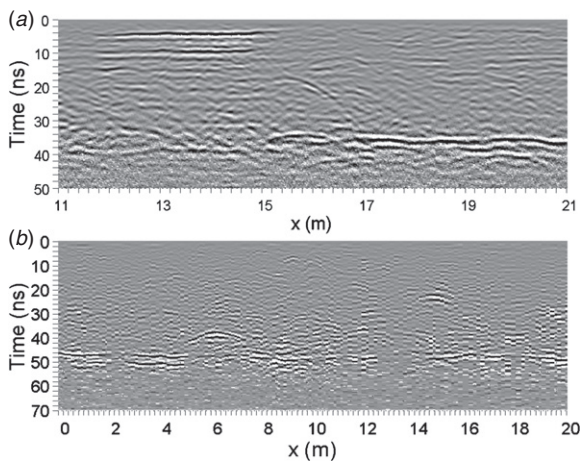


**Figure 6.** Profiles acquired at parts of the pipeline that included flanges deeper than those in the previous figures. (a) Pipeline at  $t \approx 34$  ns. The signal of the flange is hardly visible at  $(x, t) = (15.5 \text{ m}, 34 \text{ ns})$ . (b) Pipeline at  $t \approx 47$  ns. The flange signal is completely absent.

### 3.2. Pipeline depth

Figures 6(a) and (b) show radargrams obtained along deeper sections of the pipeline, which also include flanges. In these cases, the pipe was expected to be located at approximate depths of 2.4 and 3.0 m, respectively, and the flanges to be located around  $x = 15.5$  m and  $x = 9.5$  m. In figure 6(a), the signal of the pipe is clear at  $t \approx 36$  ns, but only inside the interval  $x \approx [17-21]$  m. Outside this interval the signal is very unclear because of its low amplitude, comparable to the amplitude of the surrounding signals. Absorption, divergence and shallow reflections have attenuated the fields transmitted towards and back from the pipe in this case. Also the flange signal is hardly visible in figure 6(a), with vertex at  $(x, t) = (15.5 \text{ m}, 34 \text{ ns})$ . These characteristics indicate that the penetration is to the limit in this deeper-pipe example.

In the example of figure 6(b), the signal of the pipe is located at 47 ns, approximately, presenting frequent

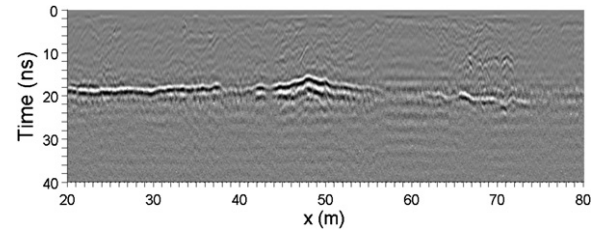


**Figure 7.** Profile acquired at a clayey sector, where there is no flange.

discontinuities along the  $x$ -interval, whereas the signal of the flange is completely absent from the radargram (the hyperbola around  $x = 6.1$  is probably due to a rock). As in the previous example, the penetration depth is clearly insufficient because of the divergence and absorption of the fields, which are important for large distances of propagation. In general, from the field tests we obtained that the detection of the flange and pipe signals was possible up to a depth of 2.0–2.5 m, depending on the sector of the pipeline. These penetrations were *a priori* sufficient to satisfactorily prospect the unknown part of the pipeline.

### 3.3. Absorbance of the soil

We also carried out a few tests in sectors that showed a clayey composition, which were distant to the studied part of the pipeline, in order to analyse how the signals behave in the presence of this material. Although there were no signs of this kind of soil along the part of the pipeline to be prospected, since the soil was predominantly sandy, these results could aid the interpretation in sectors with moderate contents of clay. Figure 7 shows a profile acquired along a clayey area. In this area the pipe is located at a depth of 1 m, approximately. It can be observed in the figure how the pipe signal is noticeably attenuated at different  $x$ -intervals because of the absorption of the GPR waves. In general, we observed that the time penetration could be as low as 7–8 ns in areas with significant amounts of clay.

### 3.4. Fluctuations in the topography and wave velocity

To evaluate the effects of the topography and velocity fluctuations on the visualization of the signals, we acquired profiles along sectors with variable topography and surface composition, corrected the profiles, and finally compared them to the originals. To maximize the contrast between the uncorrected and corrected results we clicked on the pipe signal, obtained position–time pairs and moved the traces in time according to these pairs. Although this procedure does not lead to the same result that would be obtained by correcting the topography and velocity fluctuations from experimental data, this gave us an idea of the best attainable result, and avoided obtaining both magnitudes with high precision, which would be very difficult and time consuming tasks. Figure 8(a) shows an example of an uncorrected profile, and figure 8(b) shows the corrected result. It can be observed in both figures that the flange signal is quite clear at  $x = 33.7$  m. In general, we decided not to obtain the topography and the velocity sections

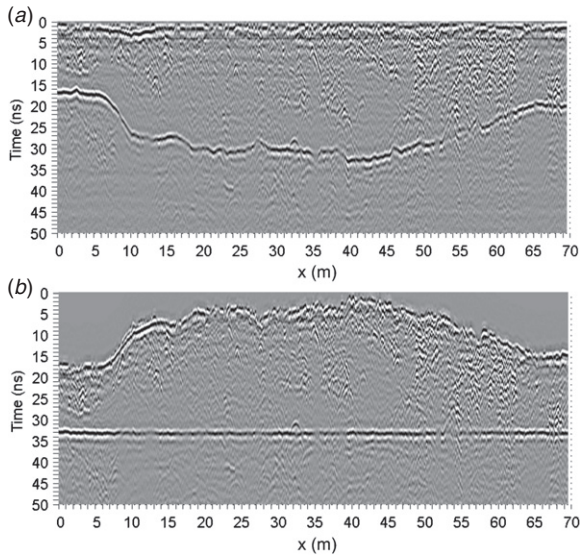


**Figure 8.** (a) Profile obtained at a sector with variable topography and surface composition; (b) corrected profile.

during the prospecting unless the *in situ* analysis, performed at the end of each day, indicated that. This significantly reduced the acquisition and processing times, and then the cost of the study.

#### 4. Fieldwork to detect the pipe flanges

The definitive fieldwork to detect the pipe flanges was performed 2 months after the field tests. A 4 day prospecting was carried out along the pipeline, which included the processing and analysis of the data at the end of each day. An additional day was necessary to mark the flange positions on the field, to excavate them and to acquire additional survey lines at a few places that presented unclear signals.

As a general methodology, we acquired consecutive profile lines along the investigated sector of the pipeline, each with a length of 100 m. Larger profiles were not acquired in order to keep the error low in the longitudinal position. We used an electromagnetic induction (EMI) device working as a metal detector to locate the pipeline trajectory along the investigated sector. Although the GPR method could also provide the transversal position with good accuracy, it would require larger times to acquire consecutive and nearby profiles across the pipeline, to process and analyse the data, and to mark the lateral positions back on the field. In contrast, the EMI system made it possible to obtain these positions directly in the field and from a single run in continuous mode. We measured and marked the trajectory at variable intervals along the pipeline, with lengths ranging from 4 to 20 m, approximately, depending on the curvature of the pipeline. This assured us a lateral deviation from the ideal trajectory below 20 cm, so that the signals of interest could be satisfactorily detected and the error in the vertical coordinate kept low enough. As in the case of the preliminary tests, we applied rubberbanding, dewow, time-zero correction, removal of the direct waves between the antennae, and exponential gain.

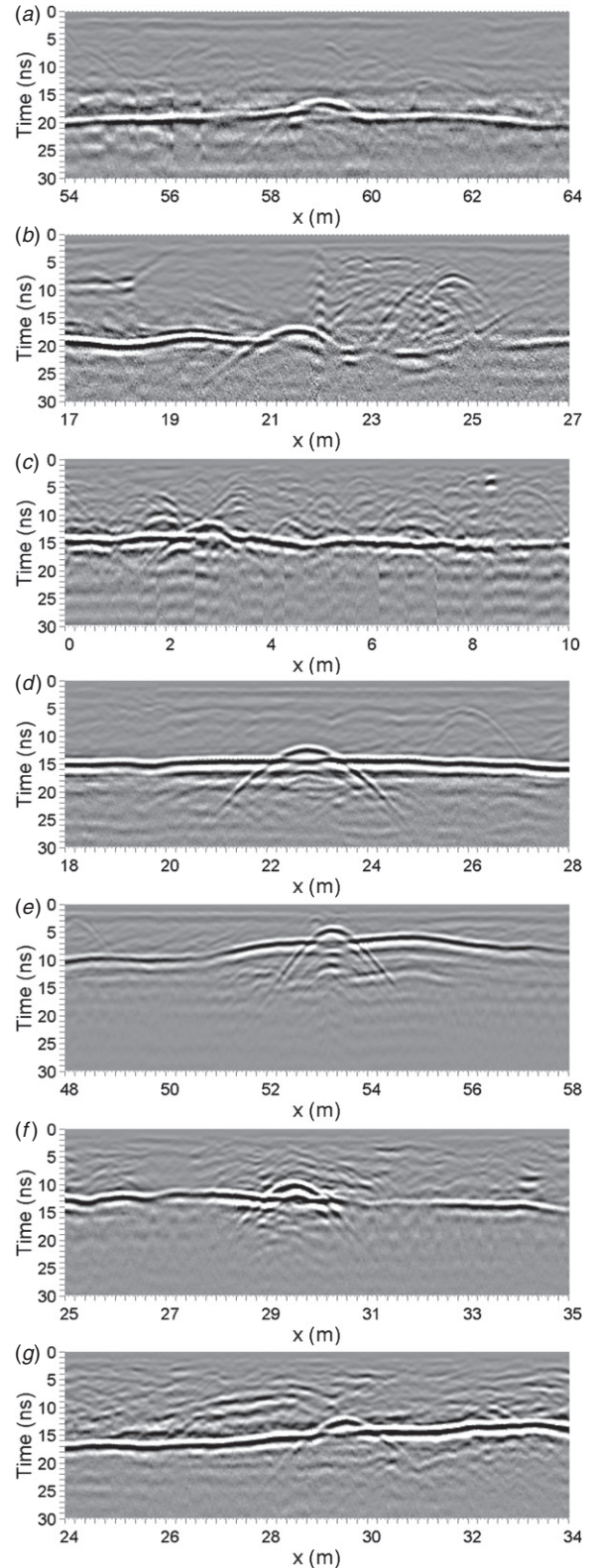


**Figure 9.** Several radargrams in which signals of flanges were detected.

In figure 9 we show several radargrams in which signals of flanges were detected. For example, a clear hyperbolic signal of a flange appears in figure 9(a) with vertex at

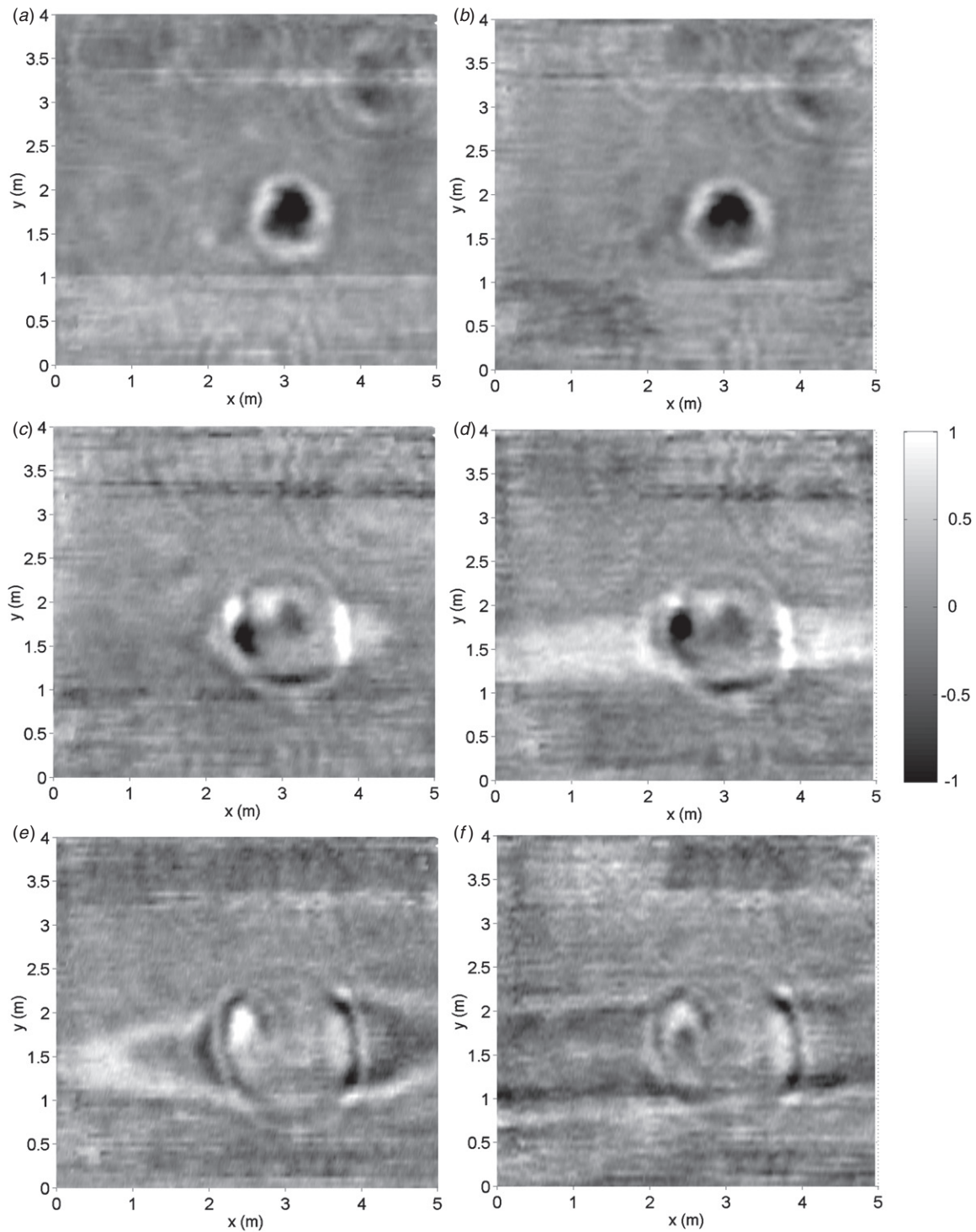


**Figure 10.** Constant-time slices obtained in the area of a confirmed flange. (a), (b)  $t = 16.0$  ns, (c), (d)  $t = 17.5$  ns and (e), (f)  $t = 19.0$  ns. In (b), (d) and (f), the topographic variations have been corrected.

$(x, t) = (59.2 \text{ m}, 16 \text{ ns})$ . In this case, the flat signal of the pipe is evident throughout the entire  $x$ -interval at  $t \approx 19$  ns. In figure 9(b), the flange signal is located at  $(x, t) = (21.6 \text{ m}, 17 \text{ ns})$ , whereas the pipe signal has become somewhat blurred along the  $x$ -intervals  $[22.9\text{--}23.6]$  and  $[24.9\text{--}25.8]$  m due to a greater dispersion in the shallower portions of soil, where appreciable fluctuations in the soil parameters occur (the

reflections that can be observed inside the area  $x = [22\text{--}25]$  m,  $t = [4\text{--}20]$  ns are consequences of these fluctuations). Lack of the signals of interest due to soil fluctuations, dispersion and absorption only occurred at short segments of the trajectory, thus not impeding the detection.

The radargram in figure 9(c) presents a number of hyperbolic signals that are located at positions compatible



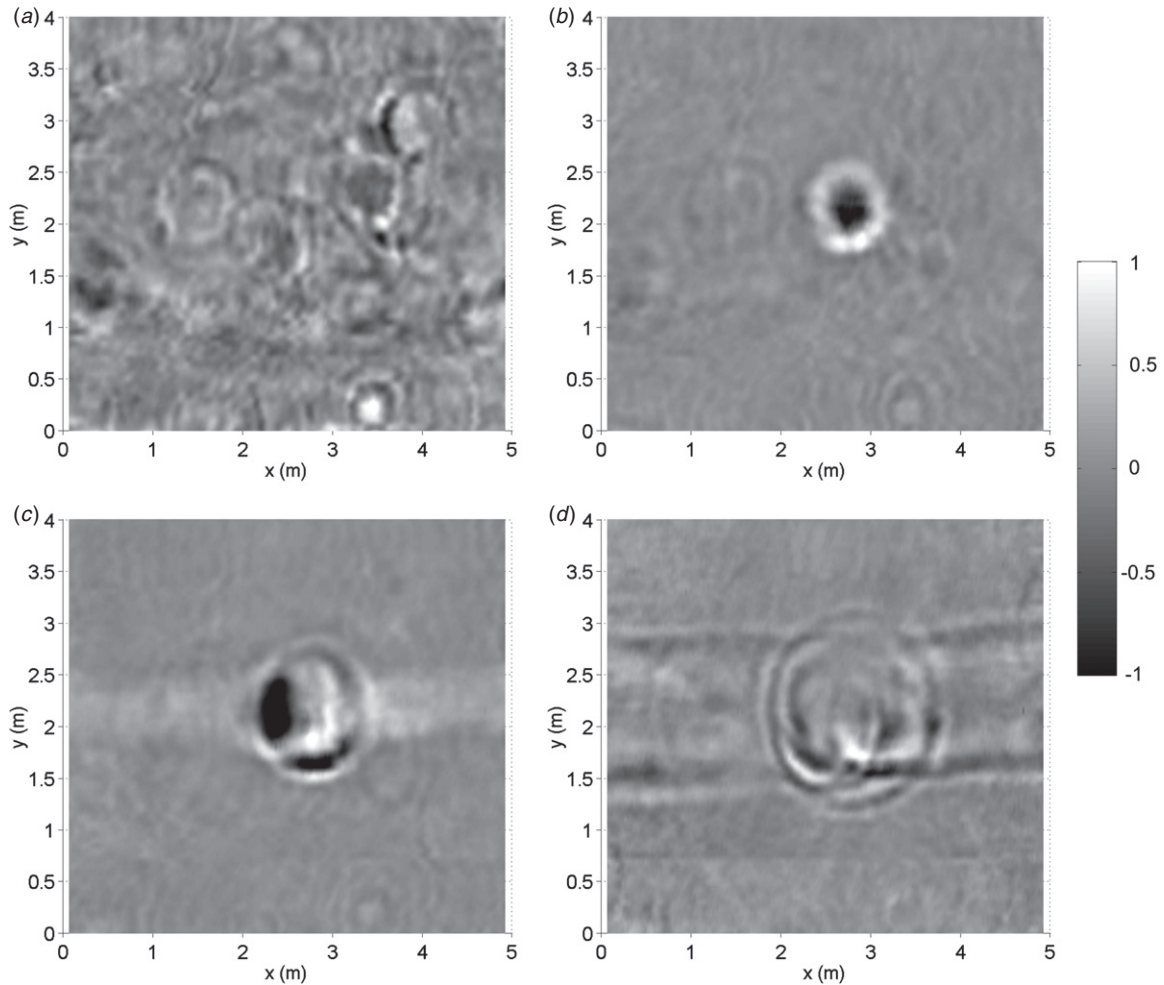


**Figure 11.** Constant-time slices obtained in the area of figure 9(c). (a)  $t = 9.0$  ns; (b)  $t = 10.5$  ns; (c)  $t = 12.0$  ns; (d)  $t = 15.0$  ns. The topography has been corrected in these figures.

with flange signals, in particular, the signals with vertices at  $(x, t) = (1.9 \text{ m}, 10.5 \text{ ns})$ ,  $(x, t) = (2.9 \text{ m}, 11.0 \text{ ns})$  and  $(x, t) = (6.9 \text{ m}, 11.0 \text{ ns})$ . Among them, the first two are more similar to flange signals than the third, mainly because the third presents too-weak intensity with respect to the pipe. In the next section, we will show how the signals of the flanges can be distinguished from other surrounding signals by performing simple additional surveys. Figures 9(d)–(g) are examples in which the flange signals can be clearly identified. As occurs with any other kind of diffraction signal, the flange signals are narrower for shallower pipelines, as in figures (e) and (f), just as a consequence of increasingly different traveltimes with respect to the minimum. Finally, some parts of the pipe signals seem to present a different phase, for example, through most of figure (a), beyond  $x = 25.8 \text{ m}$  in (b) and for  $30.6 \text{ m} < x < 32.6 \text{ m}$  in (f). These differences are only apparent (i.e. not real) and in most cases produced when the amplitude of the second maximum of the signal, which is weaker than the first maximum and the minimum between them, becomes comparable to those of the surrounding signals or below them, thus tending to

disappear. In contrast, in other parts of the radargrams, this maximum becomes more visible due to the hue saturation of the figures. Additionally, differences between the applied gain curve and the ‘ideal or exact’ curve can selectively reinforce one extreme of the pulse or the other (occasionally, making visible a small initial minimum), thus producing slight differences in the appearance of the pipe signal along the pipeline.

At the moment of prospecting we obtained a propagation velocity for the GPR waves of  $15.5 \pm 1.3 \text{ cm ns}^{-1}$ , which was higher than that obtained during the field tests,  $13.1 \pm 2.0 \text{ cm ns}^{-1}$ , probably because of a greater time interval from the rainy season to the acquisition of the data. The pipeline depths, obtained at the positions of the detected flanges, ranged from 0.5 to 1.7 m. The differences between the GPR measurements and the results of the excavations were below 10 cm for the longitudinal coordinate, and 20 cm for the vertical coordinate, whereas the accuracy in the transversal coordinate obtained with the EMI system was around 20 cm. These results indicate satisfactory precision for the applied methodology.

## 5. Analysis of constant-time slices to differentiate flange signals from other signals

From the analysis of the vertical section in figure 9(c) we could distinguish two signals that presented characteristics compatible with flange signals, although we could not relate, with enough confidence, any of them to a flange. A way to complement the available information about these signals is to obtain constant-time data slices, from which their relative positions, shapes and amplitudes can be further analysed. This analysis would make it possible to disregard signals that were not aligned with the pipeline or that presented non-circular sections. Additionally, a comparison between the doubtful signals and an experimental pattern of a flange signal would reduce the remaining uncertainty.

To obtain a confident pattern, we acquired a set of parallel closely spaced profiles at the area of a confirmed flange. Good continuity for the signals is obtained through this kind of prospecting, from which interpretation is simpler and clearer than from a few distant lines. A total of 81 lines, with length of 5 m and cross-line spacing of 5 cm, were acquired in approximately 1 h (this period includes 10 min we used to mark the area of the prospecting). Figures 10(a), (b); (c), (d) and (e), (f) show data slices for  $t \approx 16.0$ , 17.5 and 19.0 ns, respectively. In figure 10(a), the signal of the flange is clearly visible at  $(x, y) = (3.1, 1.7)$  m, while the signal of the pipe does not appear at this time due to its greater depth. Another diffraction signal, probably related to a small rock, can be observed at  $(x, y) = (4.2, 3.3)$  m. In figure 10(c), the signal from the top of the pipe appears, whereas in figure 10(e) both signals are more dispersed. In both figures the signals appear somewhat distorted due to the surface topography. Figures 10(b), (d) and (f) are analogous to figures 10(a), (c) and (e), respectively, but with the topographic variations corrected. From a comparison of these figures, it can be verified that the corrected signals are more realistic than the originals.

Figures 11(a)–(d) show constant-time slices obtained in the area of figure 9(c), for  $t \approx 9.0$ , 10.5, 12.0 and 15.0 ns, respectively. The acquisition parameters are the same as in the previous figure, and the topography has been corrected. The two doubtful signals in figure 9(c) appear in figures 11(a) and (b) centred at  $(x, y) = (1.8, 2.2)$  m and  $(x, y) = (2.8, 2.2)$  m, respectively. From a comparison of figures 11(a) and (c) it can be observed that both signals are aligned with the pipeline and present circular sections. Nevertheless, it is clear when comparing figures 11(b), (c), (d) and figures 10(b), (d), (f) that the second signal is the only one with amplitude characteristics similar to a flange signal. In contrast, the first signal is similar to other surrounding signals (figure 11(a)), which are slightly shallower than the flange signal.

To complement the analysis of the data in figures 10 and 11, we performed their 3D Stolt migrations (Stolt 1978). Figures 12(a) and (b) show constant-intensity surfaces of the migrated data. The velocity of migration has been  $v = 15.5 \text{ cm ns}^{-1}$  and  $v = 17.5 \text{ cm ns}^{-1}$ , respectively. It can be observed that both surfaces are qualitatively similar, and that their shapes approximately resemble the pipeline contour. In

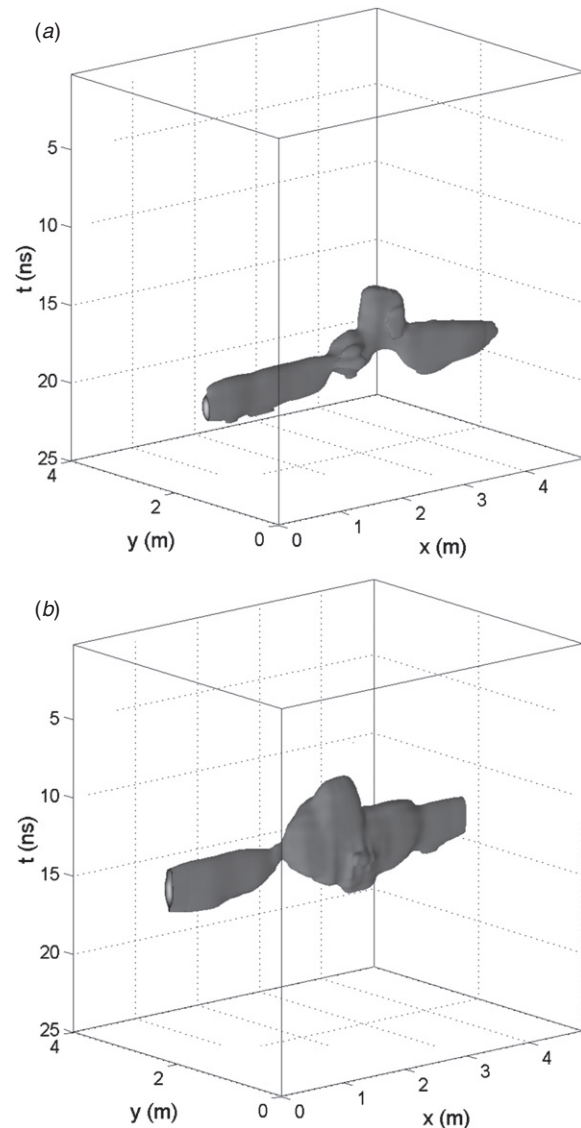


**Figure 12.** 3D Stolt migrations of the data in (a) figure 11 and (b) figure 12.

particular, in figure 12(b) the protuberance of the probable flange is located at  $(x, y) = (2.8, 2.2)$  m, at the same position as the first doubtful signal, whereas there is no protuberance at  $(x, y) = (1.8, 2.2)$  m, the position of the other doubtful signal. Then, it is also clear from this kind of representation which of the signals is probably related to a flange.

## 6. Conclusions

We have described a case history in which the ground penetrating radar method was successfully applied to locate pipe flanges along an 8 km section of a metallic pipeline, with pipe diameter of 20 cm, junction width of 20 cm and flange diameter of 56 cm. The soil surrounding the pipeline presented low humidity conditions and mainly sandy composition, with moderate contents of clays in a few segments of the pipeline trajectory.

A simple methodology for detecting and positioning the flanges was proposed and studied. In the first stage of this methodology, consecutive fixed-offset profile lines are acquired along the investigated section and from the surface of the ground. Then,  $x-t$  sections of the data are obtained, in which the signals of the pipe are located. The pipe signals are used as references to locate diffraction signals at time distances compatible with flange signals. Finally, probable flange signals are selected by comparing these signals with simulated and experimental patterns. In this manner, positions for the flanges along the pipeline are obtained. The respective vertical positions are subsequently deduced from the parameters of hyperbolic fits performed on the diffraction signals. With this methodology, the acquisition and processing times are minimal, it is not necessary to remove any portions of soil, so there is no risk of damaging the pipeline, and the normal functioning of the pipeline is unaffected.

In the first section of the paper, we showed numerical simulations performed before the field tests and definitive prospecting in order to evaluate the described methodology. We analysed which GPR frequencies would be the most suitable for resolving the signals of the pipe and the flanges during the prospecting, so that both signals could be simultaneously identified. For the considered pipeline and soil conditions, it was determined that a frequency of around 500 MHz would provide a good balance between resolution and penetration. Then, we gave estimations of the error in the measured depths when the survey line deviated from the pipeline trajectory. A depth increment of 4 cm for a typical deviation of 20 cm was obtained. We also quantified the depth increments produced by fitting hyperbolae to the signals of the flanges, since they are not punctual objects. It was established that the difference between the fitted and right depths mainly depended on the depth of the pipeline, with maximum differences of around 9 cm for the deepest parts of the pipeline (150 cm, approximately). These results were useful to correct the depths obtained during the field tests and the prospecting.

Next, we summarized field tests performed at a sector of the pipeline in which the positions of the flanges were known. Several radargrams that included pipe and flange signals were shown and analysed in order to illustrate the most relevant factors of detection. In particular we analysed the amplitude of the signals, for increasing distances between the profile line and the pipeline. It was established that for distances greater than 0.6 m the pipeline signals were too weak to be detected, mainly because of the directivity of the transmitted fields. We also determined that the detection of the pipe and flange signals was possible up to depths of around 2.0 m, which was sufficient for the unknown part of the pipeline. The attenuation of the signals at absorbing areas was also studied. The effects of the topography and velocity fluctuations on the visualization of the signals were next considered. It was shown that good visualizations could be obtained both with and without correcting these magnitudes, so it was unnecessary to measure them throughout the entire pipeline.

In the last section of the paper we showed the main results of the definitive prospecting. During the first stage of the

prospecting, we acquired 80 SO profiles along the pipeline, each 100 m long, in order to detect flange signals from a direct inspection of the radargrams. Different examples in which flange signals could be detected by applying the aforementioned methodology have been shown. Through this methodology, 85% of the expected flanges were identified during a 4 day fieldwork, at depths from 0.5 to 1.7 m. The results were checked through excavations. Mean differences of 8 cm in the longitudinal coordinate, and 10 cm for the vertical coordinate were obtained. In the remaining unclear situations, we acquired high-resolution data grids. The grids had 81 lines, with length of 5 m and cross-line spacing of 5 cm, which were acquired during approximately 1 h surveys. From these data we performed constant-time data sections and 3D migration to distinguish flange signals from other signals. This complementary methodology made possible to identify the rest of the expected flanges, which were also confirmed through later excavations. We obtained negligible horizontal error in the positioning and a vertical error of around 10 cm. In general, the errors obtained during the overall prospecting were below 10 cm for the longitudinal coordinate, and 20 cm for the vertical coordinate, close to the requirements of many utility owners, contractors and government departments (Thomas *et al* 2009).

## Acknowledgments

This work was partially supported by grants from CONICET (Consejo Nacional de Investigaciones Científicas y Técnicas) and ANPCyT (Agencia Nacional de Promoción Científica y Tecnológica).

## References

- Al-Shuhail A 2006 Mapping the surface of a shallow groundwater system using GPR: a case study in eastern Saudi Arabia *Leading Edge* **25** 738–40
- Arts R, Baradello L, Girard J, Kirby G, Lombardi S, Williamson P and Zaja A 2008 Results of geophysical monitoring over a “leaking” natural analogue site in Italy *Energy Procedia* **1** 2269–76
- Berard B and Maillol J 2008 Common- and multi-offset ground-penetrating radar study of a Roman Villa, Tourega, Portugal *Archaeological Prospection* **15** 32–46
- Bonomo N, Osella A, Cedrina L and Ratto N 2009 GPR prospecting in a prehispanic village, NW, Argentina *J. Appl. Geophys.* **67** 80–7
- Borgioli G, Capineri L, Falorni P, Matucci S and Windsor C 2008 The detection of buried pipes from time-of-flight radar data *IEEE Trans. Geosci. Remote Sens.* **46** 2254–66
- Crocco L, Prisco G, Soldovieri F and Cassidy N 2009 Early-stage leaking pipes GPR monitoring via microwave tomographic inversion *J. Appl. Geophys.* **67** 270–7
- Delle Rose M and Leucci G 2010 Towards an integrated approach for characterization of sinkhole hazards in urban environments: the unstable coastal site of Casalabate, Lecce, Italy *J. Geophys. Eng.* **7** 143–54
- Deparis J, Fricout B, Jongmans D, Villemain T, Effendiantz L and Mathy A 2008 Combined use of geophysical methods and remote techniques for characterizing the fracture network of a potentially unstable cliff site (the ‘Roche du Midi’, Vercors massif, France) *J. Geophys. Eng.* **5** 147–57

- Gomez C, Lavigne F, Hadmoko D, Lespinasse L and Wassmer P 2009 Block-and-ash flow deposition: a conceptual model from a GPR survey on pyroclastic-flow deposits at Merapi Volcano, Indonesia *Geomorphology* **110** 118–27
- Hermozilha H, Grangeia C and Matias M 2009 An integrated 3D constant offset GPR and resistivity survey on a sealed landfill—Ilhavo, NW Portugal *Int. J. Remote Sens.* **30** 2399–410
- Ho K and Gader P 2008 An investigation of using the spectral characteristics from ground penetrating radar for landmine clutter discrimination *IEEE Trans. Geosci. Remote Sens.* **46** 1177–90
- Hugenschmidt J and Kalogeropoulos A 2009 The inspection of retaining walls using GPR *J. Appl. Geophys.* **67** 335–44
- Leucci G, Persico R and Soldovieri F 2007 Detection of fractures from GPR data: the case history of the Cathedral of Otranto *J. Geophys. Eng.* **4** 452–61
- Masini N, Persico R and Rizzo E 2010 Some examples of GPR prospecting for monitoring of the monumental heritage *J. Geophys. Eng.* **7** 190–9
- Orlando L and Marchesi E 2001 Georadar as a tool to identify and characterize solid waste dump deposits *J. Appl. Geophys.* **48** 163–74
- Orlando L and Slob E 2009 Using multicomponent GPR to monitor cracks in a historical building *J. Appl. Geophys.* **67** 327–34
- Pérez-Gracia V, Caselles O, Clapés J, Osorio R, Canas J and Pujades L 2009 Radar exploration applied to historical buildings: a case study of the Marques de Llió palace, in Barcelona (Spain) *Eng. Fail. Anal.* **16** 1039–50
- Pettinelli E, Beaubien S, Lombarda S and Annan P 2008 GPR, TDR, and geochemistry measurements above an active gas vent to study near-surface gas-migration pathways *Geophysics* **73** A11–5
- Pettinelli E, Di Matteo A, Mattei E, Crocco L, Soldovieri F, Redman D and Annan P 2009 GPR response from buried pipes: measurement on field site and tomographic reconstructions *IEEE Trans. Geosci. Remote Sens.* **47** 2639–45
- Reynolds J 1997 *An Introduction to Applied and Environmental Geophysics* (Chichester: Wiley)
- Soldovieri F, Prisco G and Persico R 2008 Application of microwave tomography in hydrogeophysics: some examples *Vadose Zone J.* **7** 160–70
- Soliman M and Wu Z 2008 Buried object location based on frequency-domain UWB measurements *J. Geophys. Eng.* **5** 221–31
- Stolt R H 1978 Migration by Fourier transform *Geophysics* **43** 23–48
- Thomas A, Rogers C, Chapman D, Metje N and Castle J 2009 Stakeholder needs for ground penetrating radar utility location *J. Appl. Geophys.* **67** 345–51
- Vanneste K, Verbeeck K and Petermans Y 2008 Pseudo-3D imaging of a low-slip-rate, active normal fault using shallow geophysical methods: the Geleen fault in the Belgian Maas River valley *Geophysics* **73** B1–9
- Xie X, Liu Y, Huang H, Du J, Zhang F and Liu L 2007 Evaluation of grout behind the lining of shield tunnels using ground-penetrating radar in the Shanghai Metro Line, China *J. Geophys. Eng.* **4** 253–61
- Zeng X and McMechan G 1997 GPR characterization of buried tanks and pipes *Geophysics* **62** 797–806
- Zyadaa Z, Matsunob T, Hasegawac Y, Satoa S and Fukuda T 2009 Advances in GPR-based landmine automatic detection *J. Franklin Inst.* at press, doi:10.1016/j.jfranklin.2009.02.014